ACS Catalysis

Research Article

pubs.acs.org/acscatalysis

Mechanistic Aspects of deNO$_x$ Processing over TiO$_2$ Supported Co–Mn Oxide Catalysts: Structure–Activity Relationships and In Situ DRIFTs Analysis

Hang Hu,[†] Sixiang Cai,[†] Hongrui Li,[†] Lei Huang,[†] Liyi Shi,[†,‡] and Dengsong Zhang*[,†]

[†]Research Center of Nano Science and Technology, [‡]Department of Chemistry, Shanghai University, Shanghai 200444, China

Supporting Information

ABSTRACT: Anatase TiO$_2$-supported manganese and cobalt oxide catalysts with different Co/Mn molar ratios were synthesized by a conventional impregnation method and used for selective catalytic reduction (SCR) of NO$_x$ with NH$_3$. The catalysts were characterized by N$_2$ adsorption/desorption, X-ray diffraction, X-ray photoelectron spectroscopy, and temperature-programmed desorption with NH$_3$ and NO$_x$. Characterization of the catalyst confirmed that by using Co$_3$O$_4$ over Mn/TiO$_2$, we enhanced NO oxidation ability. From in situ diffuse reflectance infrared transform spectroscopy (DRIFTs) analysis of desorption and the transient reaction, we concluded that the addition of Co could remarkably lower the activation energy of NO$_x$ chemisorption on the catalyst surface. In addition, low-temperature SCR activity mainly results from a "fast SCR" reaction. We observed four NO$_x$ species (bidentate nitrates, gaseous NO$_2$, linear nitrites, and monodentate nitrites) on the surface of Mn/TiO$_2$ and Co–Mn/TiO$_2$ catalysts that all participated in the SCR reaction in the high temperature range. Doping of cobalt greatly improved the reactivity of gaseous NO$_2$, linear nitrites, and monodentate nitrites, which makes Co–Mn/TiO$_2$ a highly effective NH$_3$–SCR catalyst.

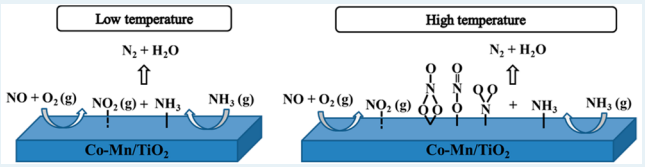

KEYWORDS: *selective catalytic reduction, cobalt oxide, TiO$_2$, in situ DRIFTs, mechanism*

1. INTRODUCTION

Over the past few decades, nitrogen oxides (NO$_x$) discharged by stationary sources and motor vehicles have been shown to be major air pollutants.[1] These pollutants are associated with a series of environmental problems, such as acid rain, photochemical smog, and ozone depletion. To control NO$_x$ emissions, several technologies have been developed, among which selective catalytic reduction with NH$_3$ (NH$_3$–SCR) is the most effective and practically applied method.[1,2] Although the V–W–TiO$_2$ catalyst, the most common commercial catalyst used, exhibits good catalytic efficiency, its high operating temperature window (300–400 °C) and the toxicity of vanadium species pose a barrier to further application. Therefore, there are several incentives to develop a vanadium-free, low-temperature deNO$_x$ catalyst system.

Recently, transition metal oxides used as catalysts have attracted attention because of their low price, high thermodynamic stability and good resistance to poisoning.[3−6] Moreover, the d shell of metal cations in transition metal oxides can easily gain and lose electrons, allowing for excellent redox properties. Manganese oxides have been shown to be an outstanding low-temperature SCR component after extensive studies.[7−11] A TiO$_2$-supported Mn-based catalyst was prepared by a conventional impregnation method that could achieve high specific surface area and facilitate the dispersion of active components, which resulted in good catalytic activity. Because of its sensitivity to impurities, a high performance catalyst was developed through suitable modifications.[12−15] Thirupathi et al.[16] prepared a series of Mn–Ni/TiO$_2$ catalysts with different Ni/Mn molar ratios and found that the doping of Ni into Mn/TiO$_2$ could change the surface Mn^{4+} concentration and that formation of this MnO$_2$ phase improved SCR performance. Similarly, a Mn–Fe/TiO$_2$ deNO$_x$ catalyst with a high chemisorbed oxygen content was prepared by deposition precipitation.[17] A Mn–Ce/TiO$_2$ catalyst has also been widely studied and showed good low-temperature catalytic activity and SO$_2$ resistance. This is mainly due to the excellent redox properties of this material.[14]

The study of the reaction mechanism is an indispensable part of understanding and designing an SCR system.[18−23] Knowledge of the reaction pathway and proposed mechanism is helpful in guiding the design and preparation of the catalyst. The feeder gas in our experiment is pure NO, but the SCR reaction varied in accordance with the proportion of NO to NO$_2$. The NO$_2$ resulted from the reaction of NO and catalyst surface active oxygen:

$$NO + O(a) \rightarrow NO_2$$

Then the so-called "fast SCR" reaction occurred:

$$NO + NO_2 + 2NH_3 \rightarrow 2N_2 + 3H_2O$$

Received: May 18, 2015
Revised: August 13, 2015
Published: September 8, 2015

DOI: 10.1021/acscatal.5b01039
ACS Catal. 2015, 5, 6069–6077

It has been reported that the "fast SCR" reaction contributes mainly to low-temperature catalytic activity.[24−28] The NO oxidation ability of the catalyst plays a critical role in the whole reaction process. In addition, NO_x will adsorb onto the catalyst surface to form different intermediates.[29−31] The participation of NO_x species with different reactivities is a clear marker needed to deduce SCR reaction pathways.

As mentioned above, the doping of Co into Mn/TiO_2 could have a positive effect on catalytic performance. Cobalt compounds have been intensively studied in many catalytic applications.[32−34] The oxidation and adsorptive ability of cobalt oxide make it a good deNO_x component.[35−37] In our previous work,[38] we synthesized $Mn_xCo_{3-x}O_4$ nanocage catalysts with good deNO_x performance. To further illuminate the promotion of NO_x reduction by Co_3O_4 with a Mn/TiO_2 catalyst, the in situ diffuse reflectance infrared transform spectroscopy (DRIFTs) technique was used to characterize the reaction intermediates and transient reaction process.

2. EXPERIMENTAL SECTION

2.1. Catalyst Preparation. The Mn/TiO_2 and Co−Mn/TiO_2 catalysts with Co/Mn molar ratios of 1, 2, 3, 4, 6, and 8 were prepared by a conventional impregnation method. Anatase TiO_2 and precursor salts $Mn(CH_3COO)_2{\cdot}4H_2O$ and $Co(CH_3COO)_2{\cdot}4H_2O$ were purchased from Sinopharm Chemical Reagent Company and used without further purification. In a typical synthesis, 20 mL of the aqueous precursor solution of $Mn(CH_3COO)_2$ and $Co(CH_3COO)_2$ was added into a 50 mL beaker containing 2.0 g TiO_2. The mixture was stirred for 3 h, dried at 80 °C for 18 h, and then calcined at 500 °C for 2 h to get the desired catalyst. The manganese loading was selected as 5 wt %, and the Co/Mn molar ratios were 1, 2, 3, 4, 6, and 8. The catalysts were denoted as Co(x)−Mn/TiO_2, where x represents the ratio of cobalt/manganese.

2.2. Catalytic Activity Evaluation. NH_3−SCR activity measurements were carried out in a fixed-bed quartz reactor (internal diameter 8 mm) using a 0.3 g sample (40−60 mesh). The following reaction conditions were used: 500 ppm of NO, 500 ppm of NH_3, 5 vol % O_2, and N_2 balance. The total flow rate was 270 mL/min, corresponding to a gas hourly space velocity (GHSV) of 40 000 h^{-1}. The concentration of the feed gases and the effluent streams were analyzed continuously by a VM4000 flue gas analyzer. The NO conversion percentage was calculated using the following equation,

$$\text{NO conversion (\%)} = \frac{[\text{NO}]_{\text{in}} - [\text{NO}]_{\text{out}}}{[\text{NO}]_{\text{in}}} \times 100\% \quad (1)$$

where the subscripts "in" and "out" denote the inlet and outlet gas concentration of the reactant, respectively.

NO oxidation and NH_3 oxidation tests were performed in the same fixed-bed quartz reactor using a 0.3 g sample. The following reaction conditions were used: 500 ppm of NO, 5 vol % O_2, and N_2 balance for NO oxidation and 500 ppm of NH_3, 5 vol % O_2, and N_2 balance for NH_3 oxidation. The total flow rate was 270 mL/min. The concentration of the feed gases and the effluent streams were analyzed continuously by a VM4000 flue gas analyzer. The NO to NO_2 conversion percentage was calculated using the following equation:

$$\text{NO-to-NO}_2\text{ conversion (\%)} = \frac{[\text{NO}_2]_{\text{out}}}{[\text{NO}]_{\text{in}}} \times 100\% \quad (2)$$

The NH_3 conversion percentage was calculated using the following equation:

$$\text{NH}_3\text{ conversion (\%)} = \frac{[\text{NH}_3]_{\text{in}} - [\text{NH}_3]_{\text{out}}}{[\text{NH}_3]_{\text{in}}} \times 100\% \quad (3)$$

By assuming that the reaction components were free of diffusion limitations, the NO oxidation rates normalized by the specific surface area of the catalyst can be calculated according to the following equation:

$$\text{rate (mmol·m}^{-2}\text{·h}^{-1}) = \frac{X_{\text{NO}} Q C_{\text{f}}}{V_{\text{m}} W S_{\text{BET}}} \quad (4)$$

where X_{NO} is the NO-to-NO_2 conversion, Q is the volumetric flow rate (mL/h), and C_f is the feeding concentration of NO (500 ppm). V_m is the molar volume of gas (22.4 mL/mmol), W is the catalyst weight (g), and S_{BET} is the specific area of the catalyst (m^2/g).

2.3. Catalyst Characterization. The specific surface areas and pore volume measurements were carried out at 77 K on a Quantachrome instrument by nitrogen adsorption/desorption. The X-ray diffraction (XRD) measurements were carried out on a computerized Rigaku D/MAS-RB X-ray diffractometer employing Cu Kα radiation operated at 40 kV and 40 mA. XRD patterns were recorded in the 2θ range of 10 to 90° at a scan rate of 8°/min. The X-ray photoelectron spectroscopy (XPS) data were obtained on an RBD upgraded PHI-5000C ESCA system with Mg Kα radiation. The binding energy of Mn, Co, and O were referenced to the C 1s line at 284.6 eV from contaminant carbon. The temperature-programmed desorption with NH_3 or NO_x (NH_3-TPD or NO_x-TPD) experiments were performed on a Tianjin XQ TP5080 autoadsorption apparatus. Prior to each experiment, the samples (150 mg) were first heated to 300 °C for 0.5 h at a ramping rate of 10 °C/min under a constant He flow rate of 30 mL/min. For NH_3-TPD, the adsorption process was carried out at 100 °C, and the samples were exposed to 500 ppm of NH_3 for 1 h, followed by He purging for 0.5 h to remove physisorbed NH_3. For NO_x-TPD, the adsorption process was carried out at 25 °C, and the samples were exposed to 500 ppm of NO + 5% O_2 for 1 h, followed by He purging for 0.5 h to remove physisorbed NO_x. During the desorption process, the samples were heated to 800 °C at a ramping rate of 10 °C/min under a flow of He (30 mL/min).

In situ DRIFTs experiments were carried out on a Nicolet 6700 spectrometer equipped with a Harrick Scientific DRIFT cell and a mercury−cadmium−telluride (MCT) detector cooled by liquid N_2. DRIFT spectra were collected in the range of 2000−800 cm^{-1}, accumulating 64 scans at 4 cm^{-1} resolution in the Kubelka−Munk format. Prior to each test, all samples were held at 300 °C under N_2 flow (50 mL/h) for 0.5 h and cooled to the desired temperature to get a background spectrum, and this spectrum was then subtracted from the sample spectra for each measurement. During the desorption process, the ramping rate is 30 °C/min, and the holding time is 1 min to collect the spectra.

3. RESULTS AND DISCUSSION

3.1. Catalytic Performance. Figure 1 shows the catalytic activity of all the prepared catalysts (Mn/TiO_2 and Co−Mn/TiO_2 catalyst with Co/Mn molar ratios = 1, 2, 3, 4, 6, 8). The results indicate that the low-temperature SCR activity of the

DOI: 10.1021/acscatal.5b01039
ACS Catal. 2015, 5, 6069−6077

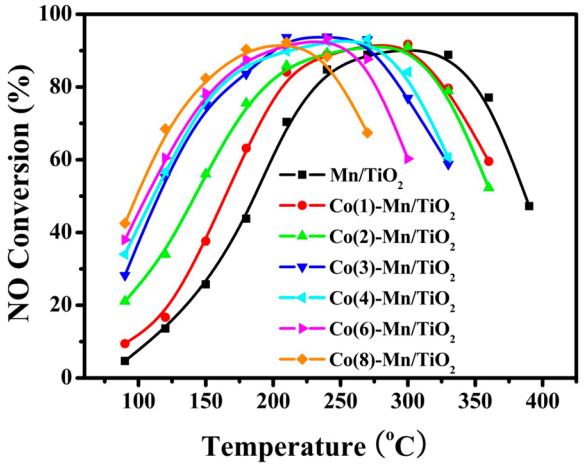

Figure 1. NO_x conversion during the NH_3–SCR reaction over Mn/TiO_2 and $Co(x)–Mn/TiO_2$ catalysts. Reaction conditions: 500 ppm of NO, 500 ppm of NH_3, 5 vol % O_2, N_2 as balance gas, total flow rate 270 mL/min, and GHSV = 40 000 h^{-1}.

$Mn–TiO_2$ catalyst was increased with an increase in Co content. This trend attenuated when the Co/Mn molar ratio was higher than 3. It was reported that the formation of NO_2 through NO oxidation over the catalyst could contribute to low-temperature activity.[21,25] We saw that the operating temperature window of each catalyst shifted to lower temperature with an increase in the Co content due to competitive ammonia oxidation. Combining all these factors, the $Co(3)–Mn/TiO_2$ was selected as the target catalyst for further study. For Co/TiO_2 catalyst with the same Co content in $Co(3)–Mn/TiO_2$ (Figure S1 in Supporting Information), the SCR activity is quite poor, which indicates that the interaction between Mn and Co results in the excellent deNO_x performance.

The properties of NO oxidation to NO_2 are illustrated in Figure 2A. With the increase of Co in the $Co–Mn/TiO_2$ catalyst, the NO oxidation ability is significantly enhanced throughout the whole temperature range. In the low temperature region (90–240 °C), the NO oxidation ability improved before the Co/Mn mole ratio reached 3, corresponding to the promotion of low-temperature activity. The NO-to-NO_2 conversion was promoted to ~10% at low-temperature range, which is consistent with the results by other researchers.[39,40] The reason for the evident difference in NO oxidation activity and low-temperature SCR activity can be attributed to the role of NH_3 during the SCR process. The NO oxidation to NO_2 is proved to be a slow step for SCR reaction,[41] whereas the generated NO_2 is rapidly consumed in the presence of NH_3. In other words, the existence of NH_3 in a real SCR reaction would increase the NO-to-NO_2 conversion when compared with the pure NO oxidation.[39]

The NO oxidation rate over Mn/TiO_2 and $Co(3)–Mn/TiO_2$ in the temperature range of 150–270 °C, where the conversion is ~30%, was calculated using eq 4. The Arrhenius plots of NO oxidation over Mn/TiO_2 and $Co(3)–Mn/TiO_2$ are shown in Figure 2B. The activation energy for NO oxidation was determined by the slope of the plot. With $Co(3)–Mn/TiO_2$, the activation energy (9.4 kJ/mol) is much lower than that on Mn/TiO_2 (21.5 kJ/mol). This result reveals that the active sites on the catalysts may have changed under these conditions; however, the NO_2 generated in large amounts at relatively high temperatures (300–420 °C) did not

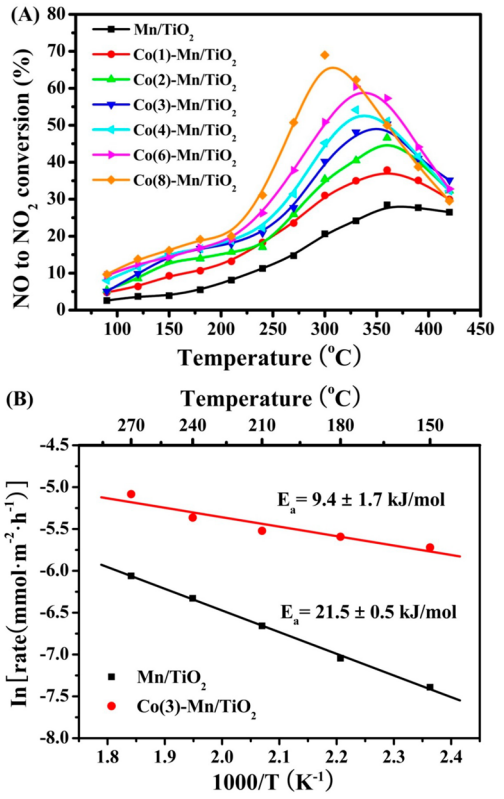

Figure 2. (A) NO-to-NO_2 conversion during the NO oxidation reaction over Mn/TiO_2 and $Co(x)–Mn/TiO_2$ catalysts. (B) Arrhenius plots of NO oxidation rates with respect to the catalyst surface over Mn/TiO_2 and $Co(3)–Mn/TiO_2$ catalysts. Reaction conditions: 500 ppm of NO, 5 vol % O_2, N_2 as balance gas, total flow rate 270 mL/min and GHSV = 40 000 h^{-1}.

contribute to SCR activity because of its deactivation mechanism.

Except for the SCR reaction, the NH_3 oxidation process over the catalyst also occurred within a relatively high temperature range, which was considered as a side reaction that would give rise to NO_x. As shown in Figure 3A, the ammonia oxidation over all the prepared catalysts increased with ramping temperature. In addition, the light-off temperature (the temperature at which the NH_3 conversion reaches 50%) gradually decreased from 245 °C (Mn/TiO_2) to 180 °C ($Co(8)–Mn/TiO_2$) with increasing Co content. This result indicates that the addition of Co promotes the oxidation ability of the catalyst, inducing the occurrence of NH_3 oxidation at lower temperatures. At the same time, the concentration of NO_x (NO and NO_2) generated during this process was monitored; these data are shown in Figure 3B. By comparing the SCR activity, we saw that NO_x formed in considerable amounts and can be seen as the main reason for catalyst deactivation. Because NH_3 oxidation will inevitably occur during the SCR process, a certain amount of reducing agent is insufficient to react with NO_x and eventually leads to catalyst deactivation.

3.2. Structure Properties. XRD was performed to determine the crystal phase of the catalyst. Figure 4 presents the XRD patterns of the $Co–Mn/TiO_2$ series catalysts. Mn/TiO_2 and $Co(1)–Mn/TiO_2$ exclusively exhibited the TiO_2 anatase crystal form. There are no diffraction peaks attributed to manganese oxides or cobalt oxides, indicating that the active

DOI: 10.1021/acscatal.5b01039
ACS Catal. 2015, 5, 6069–6077

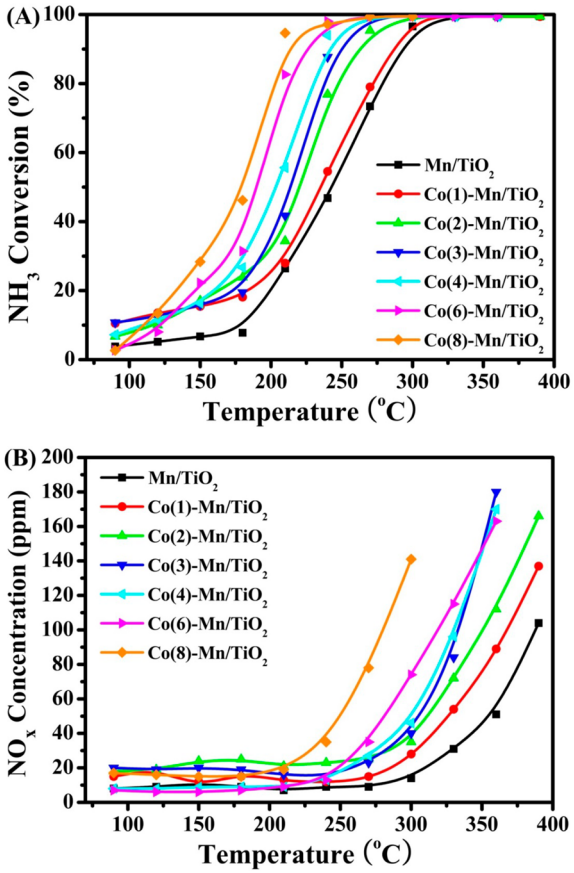

Figure 3. (A) NH_3 conversion and (B) NO_x concentration during the NH_3 oxidation reaction over Mn/TiO_2 and $Co(x)-Mn/TiO_2$ catalysts. Reaction conditions: 500 ppm of NH_3, 5 vol % O_2, N_2 as balance gas, total flow rate 270 mL/min, and GHSV = 40 000 h^{-1}.

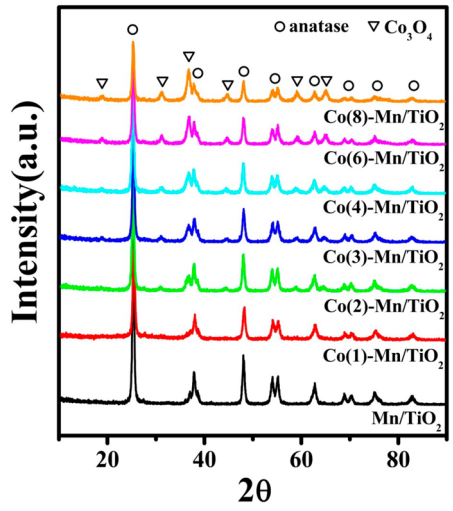

Figure 4. XRD patterns of Mn/TiO_2 and $Co(x)-Mn/TiO_2$ catalysts.

components were well dispersed on the TiO_2 support. When the Co/Mn molar ratio exceeded 1, the typical diffraction peaks of the spinel phase Co_3O_4 were observed at 2θ = 18.9°, 31.1°, 36.8°, 44.8°, 59.0°, and 65.2°, corresponding to the (111), (220), (311), (400), (511), and (440) crystal faces. With the increase in Co content, the intensity of these peaks becomes stronger.

The specific surface areas of all the catalysts derived from N_2 physisorption are summarized in Table 1. After the addition of

Table 1. Specific Surface Area and Pore Volume of Mn/TiO_2 and $Co(x)-Mn/TiO_2$ Catalysts

catalyst	surface area (m^2 g^{-1})	pore volume (cm^3 g^{-1})
Mn/TiO_2	73.2	0.45
$Co(1)-Mn/TiO_2$	56.7	0.37
$Co(2)-Mn/TiO_2$	49.1	0.33
$Co(3)-Mn/TiO_2$	51.8	0.31
$Co(4)-Mn/TiO_2$	51.3	0.28
$Co(6)-Mn/TiO_2$	43.5	0.22
$Co(8)-Mn/TiO_2$	47.1	0.20

Co into Mn/TiO_2, the specific surface area began to decrease, owing to a clogging or covering of the TiO_2 support. Considering the error of N_2 adsorption and desorption measurement, the specific surface area of the $Co(3)-Mn/TiO_2$ catalyst has no obvious difference from any other catalyst; therefore, the small difference in specific surface area is not the main factor that could influence the catalytic performance of catalyst.

3.3. XPS. To further examine the catalyst surface for $Co-Mn/TiO_2$ series catalysts and to determine the oxidation state of the metal elements and surface element concentrations, we characterized the catalyst using XPS. The XPS spectra of Mn, Co, and O are shown in Figure 5, and relative atomic concentrations are summarized in Table 2. The XPS spectra of Mn from different samples are shown in Figure 5A. Two distinct peaks centered at 642.0 and 653.8 eV were observed and are ascribed to Mn $2p_{3/2}$ and Mn $2p_{1/2}$, respectively. After the peak-fitting deconvolution, the Mn 2p XPS peaks were divided into three characteristic peaks attributed to Mn^{2+} (640.4 eV), Mn^{3+} (642.0 eV), and Mn^{4+} (644.2 eV).[16,19] Table 2 shows that the Mn^{4+}/Mn molar ratio for $Co(3)-Mn/TiO_2$ is higher than that of other catalysts. This result demonstrates that the addition of Co changes the oxidation state of Mn on the catalyst surface, leading to the variation in the Mn^{4+} concentration. The MnO_2 phase is believed to promote SCR activity and aid in the conversion of NO to NO_2.[16]

Figure 5B shows the XPS spectra of Co compared with the $Co-Mn/TiO_2$ series catalysts. The Co $2p_{3/2}$ peak is at 780.6 eV, and the Co $2p_{3/2}$ peak is at 795.8 eV.[34,38] A satellite structure was also observed and can be ascribed to the shakeup process of Co^{2+} in the high spin state. By performing peak-fitting deconvolution, it becomes evident that the Co $2p_{3/2}$ peak has two components at 779.9 and 781.5 eV, which are Co^{3+} and Co^{2+}, respectively. The spin orbit splitting is ΔE = 15.2 eV for the $2p_{3/2}$-to-$2p_{1/2}$ peak area.[38,42] As shown in Table 2, we observed an increase in surface atomic concentrations for Co due to the increased Co content in the catalyst. The relative concentration ratio of Co^{3+}/Co in $Co(3)-Mn/TiO_2$ is the highest among these catalysts. The cation distribution of the stoichiometric spinel, Co_3O_4, has been demonstrated to be $Co^{2+}[Co^{3+}]_2O_4$, and the Co^{3+} species resulted in more anionic defects. This has been shown to bring excess surface oxygen and facilitate gas molecular adsorption.[43]

The XPS spectra of O 1s over $Co-Mn/TiO_2$ catalysts are shown in Figure 5C. The O 1s bands can be fitted into two peaks, corresponding to the surface adsorbed oxygen (denoted as O_α) at 531.6–532.0 eV and lattice oxygen (denoted as O_β)

DOI: 10.1021/acscatal.5b01039
ACS Catal. 2015, 5, 6069–6077

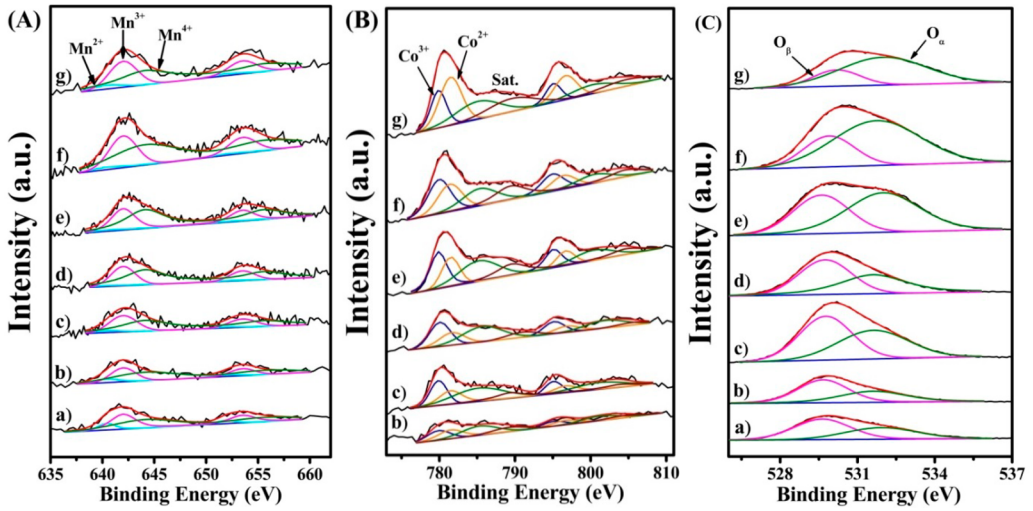

Figure 5. XPS spectra for (A) Mn 2p, (B) Co 2p, and (C) O 1s for each of the catalysts: (a) Mn/TiO_2 and (b−g) $Co(x)−Mn/TiO_2$, where x = 1, 2, 3, 4, 6, and 8, respectively.

Table 2. Surface Element Concentrations and Relative Atomic Concentrations on the Catalyst Surface

	surface atomic concentrations (%)				relative concentration ratios (%)		
catalyst	Mn	Co	O	Ti	Mn^{4+}/Mn	Co^{3+}/Co	O_α/O
Mn/TiO_2	2.46		80.48	17.03	48.70		40.70
$Co(1)−Mn/TiO_2$	2.01	1.87	77.12	19.00	56.38	46.47	41.21
$Co(2)−Mn/TiO_2$	2.01	2.01	76.18	19.74	61.01	53.55	46.10
$Co(3)−Mn/TiO_2$	2.04	2.10	75.82	20.06	64.20	61.60	46.94
$Co(4)−Mn/TiO_2$	2.28	3.15	79.19	15.36	60.73	59.03	59.46
$Co(6)−Mn/TiO_2$	2.17	3.38	79.75	14.71	58.32	55.80	71.11
$Co(8)−Mn/TiO_2$	2.22	7.68	79.34	10.76	56.94	37.00	76.45

at 529.6−530.2 eV.[34,40] As is listed in Table 2, the relative concentration ratio of O_α/O continued to rise with increasing Co content. Generally, surface adsorbed oxygen is much more reactive than lattice oxygen because of its high mobility, and therefore, it plays an important role in oxidation reactions.[34,44,45] Thus, more O_α will lead to a stronger oxidation ability, which is consistent with our NO oxidation and NH_3 oxidation results. NO was oxidized by the surface adsorbed oxygen to form NO_2, thus facilitating the "fast SCR" process.[5,21,41] However, the excessive oxidation ability has a double-edged effect because it will bring about strong ammonia oxidation. Once the reducing agent NH_3 is rapidly consumed by O_2, the SCR reaction cannot be carried out normally. The NH_3 oxidation process could even give rise to nitrogen oxide byproducts, which will narrow the window of operating temperatures.

3.4. Adsorption Proprieties. The adsorption behavior of the catalyst is considered a crucial step in a heterogeneous catalysis system. The adsorption status of the reactant gas on the catalyst surface will have a bearing on the degree of molecular activation and the catalysis process. Therefore, the adsorption of NH_3 and NO + O_2 on each catalyst was studied. The TPD technique was mainly preformed to quantify the adsorptive amounts, whereas in situ DRIFTs was used to qualify the adsorption form of the gas.

The NH_3-TPD results (Figure 6A) show that all catalysts exhibited a broad desorption peak between 150 and 400 °C, indicating that there were abundant acid sites on the Mn/TiO_2 and $Co−Mn/TiO_2$ catalysts. After the quantification of the NH_3 adsorption amount over each catalyst (Supporting

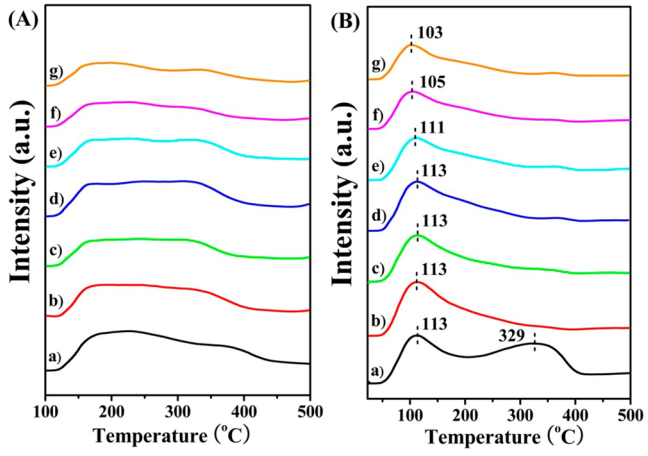

Figure 6. (A) NH_3-TPD and (B) NO_x-TPD profiles of the catalysts: (a) Mn/TiO_2 and (b−g) $Co(x)−Mn/TiO_2$, where x = 1, 2, 3, 4, 6, and 8, respectively.

Information Figure S5), it can be seen that the total acid sites on Mn/TiO_2 is the largest. With the increase in the Co content in the samples, the acid sites declined to some extent, but the $Co(3)−Mn/TiO_2$ catalyst obtained a relatively high number of acid sites among these $Co−Mn/TiO_2$ samples. The Co content continues to increase while the total NH_3 adsorption amounts shrink steadily. The NH_3 absorbed on the catalyst can further react with NO_x species to give nitrogen. The DRIFT spectra of NH_3 desorption over Mn/TiO_2 and $Co(3)−Mn/TiO_2$ are shown in Figure 7A,B. The broad peaks

DOI: 10.1021/acscatal.5b01039
ACS Catal. 2015, 5, 6069−6077

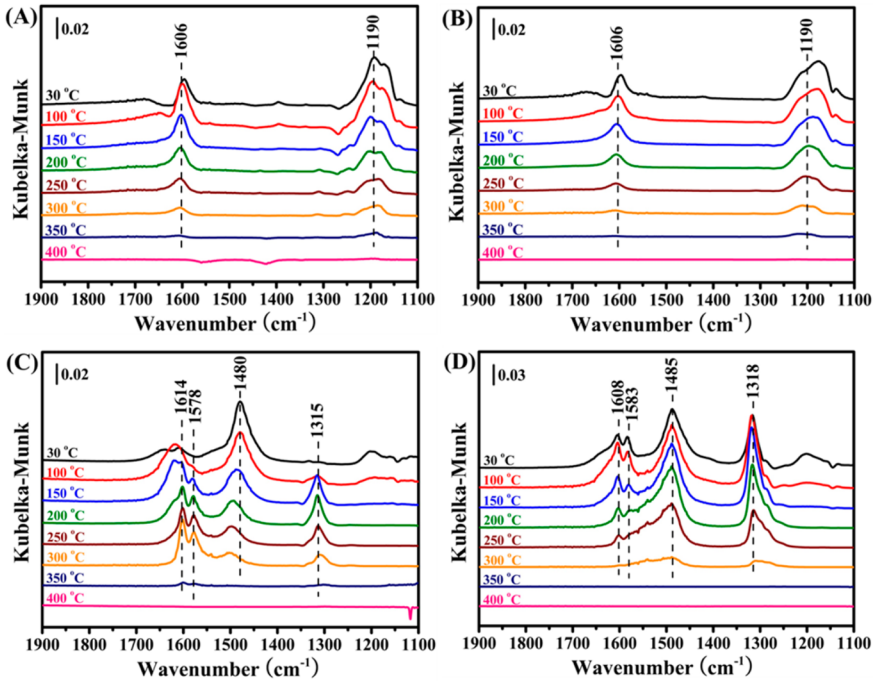

Figure 7. In situ DRIFT spectra of NH_3 desorption on (A) Mn/TiO_2 and (B) $Co(3)–Mn/TiO_2$ as a function of temperature after the catalysts were exposed to a flow of 500 ppm of NH_3 for 60 min. In situ DRIFT spectra of NO_x desorption on (C) Mn/TiO_2 and (D) $Co(3)–Mn/TiO_2$ as a function of temperature after the catalysts were exposed to a flow of 500 ppm of NO + 5% O_2 for 60 min.

centered at 1606 and 1190 cm^{-1} were assigned to the asymmetric and symmetric bending vibrations of NH_3 coordinated with Lewis acid sites.[13,19,46] The intensity of the bands from both samples showed a steady decrease until the peaks totally disappeared at 400 °C. These results indicate that the NH_3 adsorbed on the catalyst exists mainly in the form of coordinated NH_3. In addition, this type of ammonia, exhibiting strong stability, can adsorb to the catalyst surface and participate in the SCR reaction.[45]

During the adsorption of NO_x, a mixture of 500 ppm of NO and 5% O_2 will come to the catalyst surface via physical adsorption with low energy and then begin chemisorption, leading to the appearance of NO_x species.[29,31] The key factor that can directly influence the chemisorption process is the activation energy. It is evident from the NO_x-TPD results shown in Figure 6B that two desorption peaks were detected over the Mn/TiO_2 catalyst. The peak centered at 113 °C is attributed to the decomposition of surface nitrites or NO_2 desorption, and the peak at 329 °C is assigned to the decomposition of bidentate nitrates.[31,40] However, only one desorption peak at about 110 °C was detected over a series of $Co–Mn/TiO_2$ catalysts. This remarkable change of NO_x adsorption behavior can also supported by DRIFT spectra of NO_x desorption. As shown in Figure 7C, an obvious band at 1480 cm^{-1}, attributed to the ν_3 stretch vibration of linear nitrites, was detected on the Mn/TiO_2 surface at 30 °C. Along with the increase in temperature (or given energy), the bands at 1614, 1578, and 1315 cm^{-1} formed and are assigned to the asymmetric stretching vibration of gaseous NO_2, one of the split ν_3 vibrations of bidentate nitrates, and the ν_3 stretch vibration of monodentate nitrites, respectively.[13,29,47−53] While on the $Co(3)–Mn/TiO_2$ surface at 30 °C (Figure 7D), all four of the NO_x species were detected, confirming that the activation energy of chemisorption over the $Co(3)–Mn/TiO_2$ surface is significantly lower than over pure Mn/TiO_2. It is this low activation energy that leads to the formation of surface NO_x species. Among these species, the NO_2 generated at lower temperatures is promoted, and this explains why the other species contributed to the SCR activity.

3.5. Transient Reaction Studies by In Situ DRIFTs.

Transient reaction studies characterized by in situ DRIFT spectra were performed to identify reactive species and deduce a possible reaction mechanism. The DRIFT spectra of Mn/TiO_2 for the reaction between NO + O_2 and preadsorbed NH_3 at 150 and 270 °C are shown in Figure 8. After the adsorption of 500 ppm of NH_3 for 1 h, two bands at 1606 and 1190 cm^{-1} appeared and are attributed to coordinated NH_3 species. After NO + O_2 was introduced, the coordinated NH_3 was consumed to a small degree at 150 °C, which indicates that the SCR reaction did not occur. In contrast, at 270 °C, the adsorbed

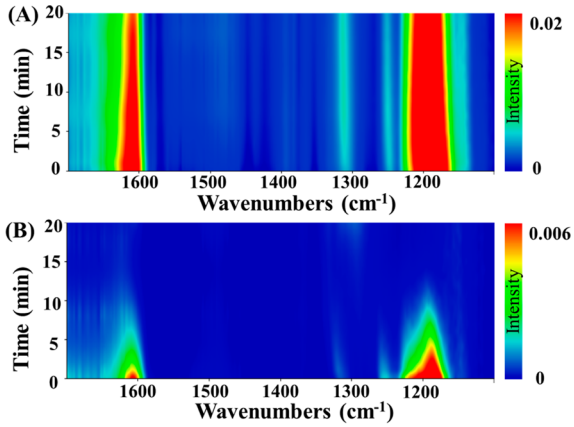

Figure 8. In situ DRIFT spectra of the transient reactions at (A) 150 °C and (B) 270 °C between NO + O_2 and preadsorbed NH_3 species over the Mn/TiO_2 catalyst recorded as a function of time.

DOI: 10.1021/acscatal.5b01039
ACS Catal. 2015, 5, 6069−6077

NH_3 decreased sharply until it totally disappeared at 10 min. This result confirms that Mn/TiO_2 exhibits good catalytic activity at 270 °C, which is consistent with our catalytic activity evaluation.

Strictly speaking, the decrease in the intensity in the characteristic peaks occurs in two parts: one is the consumption caused by the reaction, and the other is desorption from the catalyst surface. To eliminate the effect of desorption, the NH_3 or NO + O_2 preadsorbed samples were treated at 270 °C under a flow of N_2 (50 mL/min) and recorded as a function of time. The DRIFT spectra for desorption are given in Supporting Information Figures S12–S15. From these data, we saw that the decrease caused by desorption is much slower than that caused by reaction.

Figure 9 shows the DRIFT spectra for $Co(3)–Mn/TiO_2$ catalyzing the reaction between NO + O_2 and preadsorbed

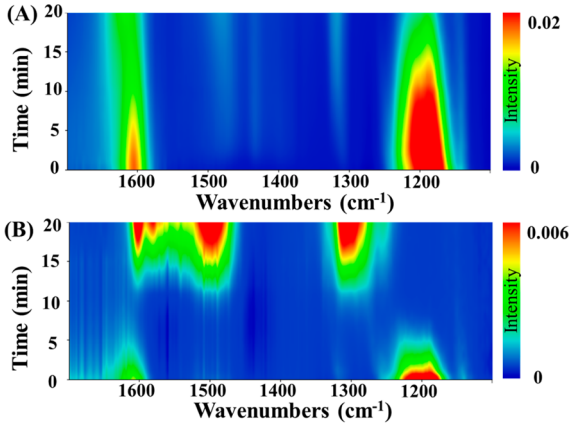

Figure 9. In situ DRIFT spectra of the transient reactions at (A) 150 °C and (B) 270 °C between NO + O_2 and preadsorbed NH_3 species over the $Co(3)–Mn/TiO_2$ catalyst recorded as a function of time.

NH_3 at 150 and 270 °C. The NH_3 preadsorption leads to the formation of the bands at 1606 and 1190 cm^{-1}, which are attributed to coordinated NH_3 species. After NO + O_2 was introduced, the intensity of the bands attributed to coordinated NH_3 decreased at 150 °C, indicating that the adsorbed NH_3 can react with NO + O_2. When the reaction temperature increased from 150 to 270 °C, the characteristic peak for coordinated NH_3 disappeared in 5 min, indicating there is a fast reaction between the NH_3 and NO + O_2. This corresponds to its excellent SCR activity. Along with the introduction of the NO + O_2, the bands at 1604, 1579, 1498, and 1311 cm^{-1} appeared and are attributed to gaseous NO_2, bidentate nitrates, linear nitrites, and monodentate nitrites, respectively. From these results, we can conclude that the NH_3 adsorbed on the catalyst surface mainly in the form of coordinated NH_3 that participates in the SCR reaction.[45]

Study of the reactivity of different NO_x species is important because the adsorption of NO + O_2 will produce multiple intermediates. The Mn/TiO_2 catalyst was first treated with 500 ppm of NO + 5% O_2 for 1 h (Figure 10), leading to the formation of the bands at 1604, 1578, 1498, and 1311 cm^{-1}, which are ascribed to gaseous NO_2, bidentate nitrates, linear nitrites, and monodentate nitrites, respectively. After 500 ppm of NH_3 was introduced, the bands due to coordinated NH_3 accumulation soon appeared at 1606 and 1190 cm^{-1}. Of those bands, the former band rapidly covered the characteristic peak of gaseous NO_2 at 1604 cm^{-1}. The bands at 1578 and 1311 cm^{-1} corresponding to bidentate nitrates and monodentate nitrites remain stable on the catalyst surface, whereas the band at 1498 cm^{-1} corresponding to linear nitrites decreases slightly, mainly as a result of its unstable structure.[29,47] These results indicate that these three NO_x species did not react with the NH_3 at 150 °C. When the transient reaction took place at 270 °C, the bands attributed to different NO_x species decreased as time went by, suggesting that the adsorbed NO_x species were consumed by ammonia and contribute to the SCR activity.

To compare the reactivity of four NO_x species—gaseous NO_2, bidentate nitrates, linear nitrites, and monodentate nitrites—the normalized band intensity of the different species at 270 °C was recorded as a function of time and is shown in Figure 10C. The reactivity of NO_x species on Mn/TiO_2 at 270 °C decreased in the following sequence: bidentate nitrates > gaseous NO_2 > linear nitrites > monodentate nitrites. These results show that the fast SCR reaction with NO_2 still occurs, but NO_2 is not the only reactive species at a relatively high temperature. In previous studies, Kijlstra et al.[54] made a similar conclusion, suggesting that the bidentate nitrates were able to react above 500 K. In addition, a transient isotopic labeling technique was used to investigate the mechanism, and it was found that the bidentate nitrates could react with NH_3 on Lewis acid sites via rearrangement.[55]

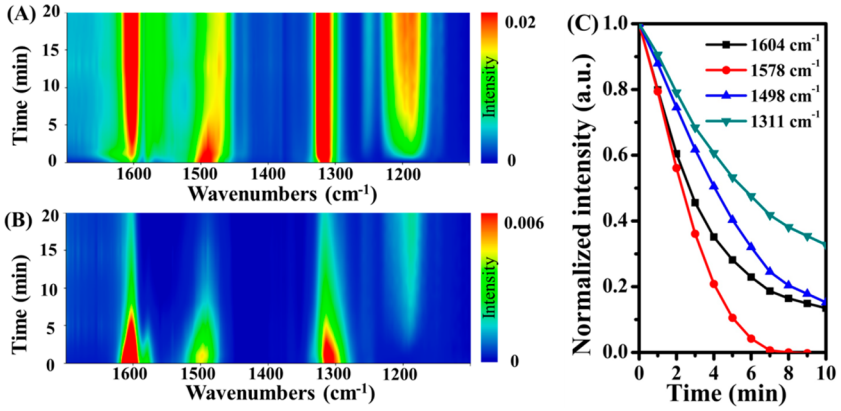

Figure 10. In situ DRIFT spectra of the transient reactions at (A) 150 °C and (B) 270 °C between NH_3 and preadsorbed NO + O_2 species over the Mn/TiO_2 catalyst recorded as a function of time. (C) Consumption of different NO_x species at 270 °C upon passing NH_3 over NO + O_2-preadsobed Mn/TiO_2 catalyst.

DOI: 10.1021/acscatal.5b01039
ACS Catal. 2015, 5, 6069–6077

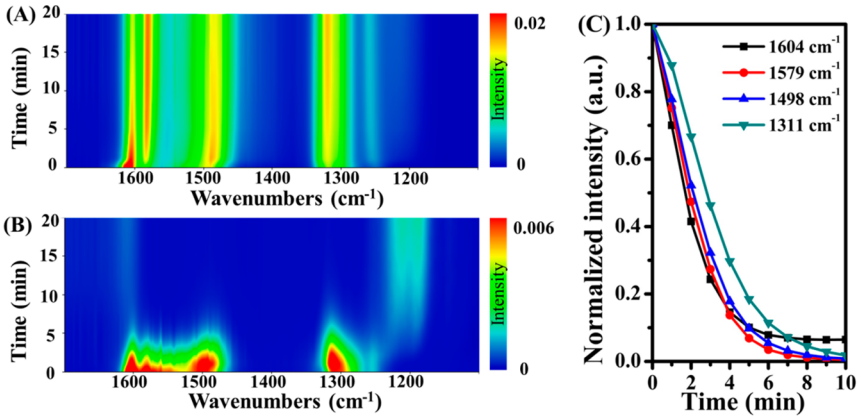

Figure 11. In situ DRIFT spectra of the transient reactions at (A) 150 °C and (B) 270 °C between NH_3 and preadsorbed NO + O_2 species over the Co(3)−Mn/TiO_2 catalyst recorded as a function of time. (C) Consumption of different NO_x species at 270 °C upon passing NH_3 over NO + O_2-preadsobed Co(3)−Mn/TiO_2 catalyst.

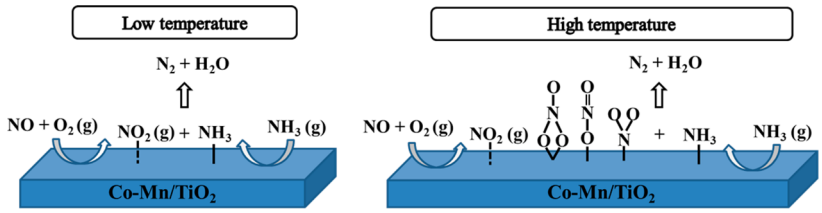

Figure 12. Proposed reaction mechanism of NH_3−SCR of NO over a Co−Mn/TiO_2 catalyst surface.

For the Co(3)−Mn/TiO_2 catalyst (Figure 11), the adsorption of NO + O_2 also leads to the formation of four NO_x species: gaseous NO_2 (1604 cm^{-1}), bidentate nitrates (1579 cm^{-1}), linear nitrites (1498 cm^{-1}), and monodentate nitrites (1311 cm^{-1}). After NH_3 was introduced, only the band attributed to gaseous NO_2 started to decrease. Meanwhile, the characteristic peak of coordinated NH_3 did not appear, which confirms that NO_2 and NH_3 participate in the fast SCR reaction and the catalysts show good low-temperature catalytic performance. Another important factor having a dramatic impact on this occurrence is the activation energy of fast SCR reaction. From the DRIFTs result of the transient reaction between NH_3 and preadsorbed NO_x over the Mn/TiO_2 catalyst at 150 °C mentioned above, even though the gaseous NO_2 formed on the catalyst, the fast SCR reaction actually did not occur; therefore, the interaction of Co with Mn plays a role in reducing the activation energy needed to start this reaction.

When the transient reaction occurred at 270 °C, all the NO_x species diminished quickly, giving proof that gaseous NO_2, bidentate nitrates, linear nitrites, and monodentate nitrites on the Co(3)−Mn/TiO_2 catalyst surface took part in the SCR reaction. This also demonstrates the excellent deNO_x activity of these species. After the NO_x was completely consumed, the bands attributed to coordinated NH_3 appeared. Similarly, the normalized intensity changed with time from different NO_x species, as shown in Figure 11C. It can be seen that the consumption of gaseous NO_2, bidentate nitrates and linear nitrites is very fast, and that of monodentate nitrites is slightly slower. Compared with the Mn/TiO_2 catalyst, the reactivity of bidentate nitrates on both catalysts is about the same, whereas the reactivity of gaseous NO_2, bidentate nitrates and monodentate nitrites is greatly improved by the addition of Co. Therefore, the interaction of Co and Mn is believed to increase the reaction rate between these NO_x species and NH_3.

The possible reaction pathway for selective catalytic reduction of NO with NH_3 over the Co−Mn/TiO_2 catalyst is proposed in Figure 12. The NO_x first adsorbed on the catalyst surface to form four kinds of NO_x species: gaseous NO_2, bidentate nitrates, linear nitrites, and monodentate nitrites, whereas reactant gas NH_3 adsorbed on Lewis acid sites in the form of coordinated NH_3. At low temperatures, only gaseous NO_2 participates in the catalytic reaction as a "fast SCR" reaction intermediate. In contrast, all of the NO_x species can rapidly react with coordinated NH_3 to give N_2 at high temperatures.

4. CONCLUSIONS

In this study, a series of Co−Mn/TiO_2 catalysts were prepared by an impregnation method for selective catalytic reduction of NO with NH_3. Among them, the Co(3)−Mn/TiO_2 catalyst exhibits excellent low-temperature catalytic activity with a broad operating temperature window. The Co promotes low-temperature activity and generates more NO_2 through NO oxidation. It also lowers the activation energy of NO oxidation and NO_x chemisorption over the catalyst. The reactivity of NO_x species on the Mn/TiO_2 catalyst in the high temperature range is as follows: bidentate nitrates > gaseous NO_2 > linear nitrites > monodentate nitrites. The addition of Co could remarkably lower the activation energy of the "fast SCR" reaction at low temperatures. In addition, the reactivity of gaseous NO_2, linear nitrites and monodentate nitrites was greatly improved at high temperature, leading to an increase in the deNO_x efficiency; however, the operating temperature window was narrowed by the excess cobalt species in Co−Mn/TiO_2, which can induce strong ammonia oxidation. Therefore, the appropriate proportion of cobalt and manganese is very important in preparing a highly effective NH_3−SCR catalyst.

DOI: 10.1021/acscatal.5b01039
ACS Catal. 2015, 5, 6069−6077

■ ASSOCIATED CONTENT

Supporting Information

The Supporting Information is available free of charge on the ACS Publications website at DOI: 10.1021/acscatal.5b01039.

Preparation, catalytic performances and characterizations of Co/TiO_2 catalyst; stability test and H_2O tolerance tests of the catalysts; the 2D in situ DRIFT spectra of desorption and transient reaction (PDF)

■ AUTHOR INFORMATION

Corresponding Author

*E-mail: dszhang@shu.edu.cn.

Notes

The authors declare no competing financial interest.

■ ACKNOWLEDGMENTS

The authors acknowledge the support of the National Basic Research Program of China (973 Program, 2014CB660803), the National Natural Science Foundation of China (U1462110), the Science and Technology Commission of Shanghai Municipality (13NM1401200), and the Shanghai Municipal Education Commission (14ZZ097).

■ REFERENCES

(1) Topsoe, N.-Y. *Science* **1994**, *265*, 1217−1219.
(2) Mou, X.; Zhang, B.; Li, Y.; Yao, L.; Wei, X.; Su, D. S.; Shen, W. *Angew. Chem., Int. Ed.* **2012**, *51*, 2989−2993.
(3) Peña, D. A.; Uphade, B. S.; Smirniotis, P. G. *J. Catal.* **2004**, *221*, 421−431.
(4) Zhou, G.; Zhong, B.; Wang, W.; Guan, X.; Huang, B.; Ye, D.; Wu, H. *Catal. Today* **2011**, *175*, 157−163.
(5) Shu, Y.; Sun, H.; Quan, X.; Chen, S. *J. Phys. Chem. C* **2012**, *116*, 25319−25327.
(6) Qu, R.; Gao, X.; Cen, K.; Li, J. *Appl. Catal., B* **2013**, *142−143*, 290−297.
(7) Yu, J.; Guo, F.; Wang, Y.; Zhu, J.; Liu, Y.; Su, F.; Gao, S.; Xu, G. *Appl. Catal., B* **2010**, *95*, 160−168.
(8) Tang, N.; Liu, Y.; Wang, H.; Wu, Z. *J. Phys. Chem. C* **2011**, *115*, 8214−8220.
(9) Ettireddy, P. R.; Ettireddy, N.; Mamedov, S.; Boolchand, P.; Smirniotis, P. G. *Appl. Catal., B* **2007**, *76*, 123−134.
(10) Shi, Y.; Chen, S.; Sun, H.; Shu, Y.; Quan, X. *Catal. Commun.* **2013**, *42*, 10−13.
(11) Maitarad, P.; Zhang, D.; Gao, R.; Shi, L.; Li, H.; Huang, L.; Rungrotmongkol, T.; Zhang, J. *J. Phys. Chem. C* **2013**, *117*, 9999−10006.
(12) Thirupathi, B.; Smirniotis, P. G. *Appl. Catal., B* **2011**, *110*, 195−206.
(13) Liu, Z.; Zhang, S.; Li, J.; Ma, L. *Appl. Catal., B* **2014**, *144*, 90−95.
(14) Jin, R.; Liu, Y.; Wang, Y.; Cen, W.; Wu, Z.; Wang, H.; Weng, X. *Appl. Catal., B* **2014**, *148−149*, 582−588.
(15) Yang, S.; Wang, C.; Ma, L.; Peng, Y.; Qu, Z.; Yan, N.; Chen, J.; Chang, H.; Li, J. *Catal. Sci. Technol.* **2013**, *3*, 161−168.
(16) Thirupathi, B.; Smirniotis, P. G. *J. Catal.* **2012**, *288*, 74−83.
(17) Putluru, S. S. R.; Schill, L.; Jensen, A. D.; Siret, B.; Tabaries, F.; Fehrmann, R. *Appl. Catal., B* **2015**, *165*, 628−635.
(18) Busca, G.; Lietti, L.; Ramis, G.; Bert, F. *Appl. Catal., B* **1998**, *18*, 1−36.
(19) Yang, S.; Wang, C.; Li, J.; Yan, N.; Ma, L.; Chang, H. *Appl. Catal., B* **2011**, *110*, 71−80.
(20) Liu, F.; Yu, Y.; He, H. *Chem. Commun.* **2014**, *50*, 8445−8463.
(21) Long, R. Q.; Yang, R. T. *J. Catal.* **2002**, *207*, 224−231.
(22) Zhang, L.; Pierce, J.; Leung, V. L.; Wang, D.; Epling, W. S. *J. Phys. Chem. C* **2013**, *117*, 8282−8289.
(23) Wang, D.; Zhang, L.; Kamasamudram, K.; Epling, W. S. *ACS Catal.* **2013**, *3*, 871−881.
(24) Wang, W.; McCool, G.; Kapur, N.; Yuan, G.; Shan, B.; Nguyen, M.; Graham, U. M.; Davis, B. H.; Jacobs, G.; Cho, K.; Hao, X. *Science* **2012**, *337*, 832−835.
(25) Tronconi, E.; Nova, I.; Ciardelli, C.; Chatterjee, D.; Weibel, M. *J. Catal.* **2007**, *245*, 1−10.
(26) Pérez Vélez, R.; Ellmers, I.; Huang, H.; Bentrup, U.; Schünemann, V.; Grünert, W.; Brückner, A. *J. Catal.* **2014**, *316*, 103−111.
(27) Yoon, D. Y.; Lim, E.; Kim, Y. J.; Kim, J. H.; Ryu, T.; Lee, S.; Cho, B. K.; Nam, I.-S.; Choung, J. W.; Yoo, S. *J. Catal.* **2014**, *319*, 182−193.
(28) Grossale, A.; Nova, I.; Tronconi, E.; Chatterjee, D.; Weibel, M. *J. Catal.* **2008**, *256*, 312−322.
(29) Hadjiivanov, K. I. *Catal. Rev.: Sci. Eng.* **2000**, *42*, 71−144.
(30) Kwak, J. H.; Lee, J. H.; Burton, S. D.; Lipton, A. S.; Peden, C. H.; Szanyi, J. *Angew. Chem., Int. Ed.* **2013**, *52*, 9985−9989.
(31) Ma, L.; Cheng, Y.; Cavataio, G.; McCabe, R. W.; Fu, L.; Li, J. *Appl. Catal., B* **2014**, *156−157*, 428−437.
(32) Xie, X.; Li, Y.; Liu, Z. Q.; Haruta, M.; Shen, W. *Nature* **2009**, *458*, 746−749.
(33) Tyo, E. C.; Yin, C.; Di Vece, M.; Qian, Q.; Kwon, G.; Lee, S.; Lee, B.; DeBartolo, J. E.; Seifert, S.; Winans, R. E.; Si, R.; Ricks, B.; Goergen, S.; Rutter, M.; Zugic, B.; Flytzani-Stephanopoulos, M.; Wang, Z. W.; Palmer, R. E.; Neurock, M.; Vajda, S. *ACS Catal.* **2012**, *2*, 2409−2423.
(34) Bai, B.; Arandiyan, H.; Li, J. *Appl. Catal., B* **2013**, *142−143*, 677−683.
(35) Wang, L.; Zhang, S.; Zhu, Y.; Patlolla, A.; Shan, J.; Yoshida, H.; Takeda, S.; Frenkel, A. I.; Tao, F. *ACS Catal.* **2013**, *3*, 1011−1019.
(36) Irfan, M. F.; Goo, J. H.; Kim, S. D. *Appl. Catal., B* **2008**, *78*, 267−274.
(37) He, C.; Kohler, K. *Phys. Chem. Chem. Phys.* **2006**, *8*, 898−905.
(38) Zhang, L.; Shi, L.; Huang, L.; Zhang, J.; Gao, R.; Zhang, D. *ACS Catal.* **2014**, *4*, 1753−1763.
(39) Chen, Z.; Yang, Q.; Li, H.; Li, X.; Wang, L.; Chi Tsang, S. *J. Catal.* **2010**, *276*, 56−65.
(40) Guan, B.; Lin, H.; Zhu, L.; Tian, B.; Huang, Z. *Chem. Eng. J.* **2012**, *181−182*, 307−322.
(41) Long, R. Q.; Yang, R. T. *J. Catal.* **2002**, *207*, 274−285.
(42) He, T.; Chen, D.; Jiao, X.; Wang, Y.; Duan, Y. *Chem. Mater.* **2005**, *17*, 4023−4030.
(43) Meng, B.; Zhao, Z.; Wang, X.; Liang, J.; Qiu, J. *Appl. Catal., B* **2013**, *129*, 491−500.
(44) Cai, S.; Zhang, D.; Shi, L.; Xu, J.; Zhang, L.; Huang, L.; Li, H.; Zhang, J. *Nanoscale* **2014**, *6*, 7346−7353.
(45) Peng, Y.; Wang, C.; Li, J. *Appl. Catal., B* **2014**, *144*, 538−546.
(46) Liu, F.; He, H. *J. Phys. Chem. C* **2010**, *114*, 16929−16936.
(47) Kijlstra, W. S.; Brands, D. S.; Poels, E. K.; Bliek, A. *J. Catal.* **1997**, *171*, 208−218.
(48) Xu, L.; Li, X.-S.; Crocker, M.; Zhang, Z.-S.; Zhu, A.-M.; Shi, C. *J. Mol. Catal. A: Chem.* **2013**, *378*, 82−90.
(49) Schneider, H.; Scharf, U.; Wokaun, A.; Baiker, A. *J. Catal.* **1994**, *146*, 545−556.
(50) Centi, G.; Perathoner, S.; Biglino, D.; Giamello, E. *J. Catal.* **1995**, *152*, 75−92.
(51) Chen, H.; Voskoboinikov, T.; Sachtler, W. M. H. *J. Catal.* **1998**, *180*, 171−183.
(52) Sedlmair, C.; Seshan, K.; Jentys, A.; Lercher, J. A. *J. Catal.* **2003**, *214*, 308−316.
(53) Yu, J.; Jiang, Z.; Zhu, L.; Hao, Z.; Xu, Z. *J. Phys. Chem. B* **2006**, *110*, 4291−4300.
(54) Kijlstra, W. S.; Brands, D. S.; Poels, E. K.; Bliek, A. *J. Catal.* **1997**, *171*, 219−230.
(55) Ettireddy, P. R.; Ettireddy, N.; Boningari, T.; Pardemann, R.; Smirniotis, P. G. *J. Catal.* **2012**, *292*, 53−63.

DOI: 10.1021/acscatal.5b01039
ACS Catal. 2015, 5, 6069−6077